Classification
Physics Abstracts
05.40 — 46.10

Two-dimensional powder transport on a vibrating belt

J.A.C. Gallas([1,2,*]), H.J. Herrmann([1]) and S. Sokolowski([1,3])

([1]) Höchstleistungsrechenzentrum, KFA, 5170 Jülich, Germany
([2]) Laboratório de Óptica Quântica da UFSC, 88049 Florianópolis, Brazil
([3]) Department of Theoretical Chemistry, MCS University, 20031 Lublin, Poland

(Received 23 March 1992, accepted 9 April 1992)

Abstract. — The transport of 2D powder mixtures is investigated using a model recently proposed by us to describe the fluidization of granular media. We simulate the behaviour of particles placed on a belt having vertical as well as horizontal vibrations. Using Molecular Dynamics we calculate the density field and velocity distributions of the particles and investigate the angular dependence of momentum transfer. We investigate these properties as functions of friction parameters and present predictions that might be checked experimentally.

1. Introduction.

The mechanical properties of granular materials like sand or powder are quite astonishing and have been the subject of a great interest for many years. Well-known examples of such intriguing behaviour are heap formation under vibration [1 – 6], density waves emitted from outlets [7] as well as the so-called "Brazil nut" segregation [8 – 11]. All these effects seem to eventually originate in the ability of these materials to form a hybrid state between a fluid and a solid [12 – 14]. Numerous attempts have been made to formalize and qualify the rheology of granular media [15 – 20], but the knowledge of the physical principles governing the behaviour of these materials is still far from being satisfactory. Moreover, many artifacts as dilatancy, arching, segregation, etc., conspire to create hystereses and instabilities of experimental results, making their reproducibility and control difficult [13, 14, 21 – 23]. The development of analytical theories is also complicated because the boundary conditions and the distribution functions for such materials are poorly understood [14, 22, 24]. For these reasons ideally suited tools to investigate granular media are computer simulational techniques [19, 20, 25 – 32].

In a previous paper [31] we presented a model reproducing a recent experiment on fluidization of a two-dimensional packing submitted to vertical vibrations [33]. A more elaborated version of the model [32] was then applied to investigate various types of convection cells due, either to the existence of walls or to spatial modulations in the amplitude of the vibration. The

(*) *Address for* 1992: Laboratory for Plasma Research, University of Maryland, College Park, MD 20742.

purpose of this paper is to report on the application of our previously proposed model [32] to simulate the behaviour of two-dimensional granular material on a flat vibrating bottom and periodic boundary conditions in the horizontal direction. The harmonic vibrations are directed at a given angle with respect to the direction of gravity. This kind of vibrating excitation is used technologically in special conveyor belts that are used for instance in the pharmaceutical industry [34]. These vibrating conveyor belts as a means of transportation are in fact very typical for granular media, since neither solids nor fluids can be moved in this way.

The purpose of our simulations is to learn more about the microscopic nature of fluidization, and how the transport of the beads occurs, i.e. how do velocity profiles depend on the shaking and on the friction coefficients involved [34]. Such basic questions are fundamental for the understanding of many interesting and elusive phenomena displayed by granular media under more constrained conditions, either by external walls or by internal forces.

2. The model.

The system we chose to study is perhaps one of the simplest one: a collection of N spherical particles of different radii sitting on a horizontal segment of a belt of width L with periodic boundary conditions in the horizontal direction. This segment undergoes harmonic oscillations in both horizontal (x) and vertical (z) directions according to

$$x(t) = A_x \sin(2\pi f t) \tag{1a}$$

$$z(t) = A_z \sin(2\pi f t) \tag{1b}$$

where f is the frequency and A_x and A_z are x and z amplitudes, respectively. The corresponding angle of the composed oscillation is $\alpha = \arctan(A_z/A_x)$.

Our model includes the fact that dissipation of energy occurs *via* inelastic interparticle collisions as well as *via* collisions of the particles with the walls. Obviously, the real molecular mechanism of energy dissipation is very complicated and can not be treated on the same time and size scales as the collisions between beads. Therefore we approximate this mechanism in a phenomenological manner by considering dissipation due to inelasticity of the collisions, as well as dissipation due to shear friction. Thus, in our present simulations the beads are subjected to a 10 m/s^2 gravitational acceleration and three kinds of forces which act during collisions between a pair of beads i and j. The first is an elastic restoration force

$$\mathbf{f}_{\rm el}^{(\rm i)} = Y(\mid \mathbf{r}_{\rm ij} \mid -\frac{1}{2}(d_{\rm i} + d_{\rm j}))\frac{\mathbf{r}_{\rm ij}}{\mid \mathbf{r}_{\rm ij} \mid} \quad , \tag{2}$$

where $d_{\rm i}$ is the diameter of the particle i, Y the Young modulus [11, 29], and $\mathbf{r}_{\rm ij}$ points from particle i to j. The second force steems from dissipation due to the inelasticity of the collision

$$\mathbf{f}_{\rm diss}^{(\rm i)} = -\gamma m_{\rm i}(\mathbf{v}_{\rm ij} \cdot \mathbf{r}_{\rm ij})\frac{\mathbf{r}_{\rm ij}}{\mid \mathbf{r}_{\rm ij} \mid^2} \quad , \tag{3}$$

where γ is a phenomenological dissipation coefficient, $m_{\rm i} \propto d_{\rm i}^2$ the mass of the ith bead and $\mathbf{v}_{\rm ij} = \mathbf{v}_{\rm i} - \mathbf{v}_{\rm j}$ the relative velocity. Finally, the third force is a shear friction intended to indirectly mimic the effect of static friction

$$\mathbf{f}_{\rm shear}^{(\rm i)} = -\gamma_{\rm s} m_{\rm i}(\mathbf{v}_{\rm ij} \cdot \mathbf{t}_{\rm ij})\frac{\mathbf{t}_{\rm ij}}{\mid \mathbf{r}_{\rm ij} \mid^2} \quad . \tag{4}$$

In this expression $\gamma_{\rm s}$ is the shear friction coefficient and $\mathbf{t}_{\rm ij} = (-r_{\rm ij}^z, r_{\rm ij}^x)$ is the vector $\mathbf{r}_{\rm ij}$ rotated by 90°. As compared to other modelizations of the forces acting between grains [11, 26, 28, 29] our equations (2-4) are simpler since we neglect Coulomb friction and the rotation of particles; we did this on purpose in order to omit, in our opinion, unimportant fit parameters.

When a particle collides with the belt the same forces act as if it would have encountered another particle of diameter $\langle d \rangle$ at the collision point. All the constants characterizing particle-wall collisions have been assumed to be the same as those for interparticle collisions. Our calculations were carried out for a uniform mixture of spherical beads. The bead diameters were chosen with uniform probability from the interval (0.5 mm, 1.5 mm) and the average diameter was $\langle d \rangle = 1$ mm. The density of all beads was assumed to be the same.

We apply a Molecular Dynamics (MD) technique [35, 36], as has been done in previous works [31, 32]. The equations of motion have been solved numerically by using classical predictor-corrector methods with a time step $\Delta = (2000f)^{-1}$. We started simulations from a random distribution of beads, letting them fall freely under gravity without shaking at the beginning. The system was allowed to evolve until the averaged squared velocity per bead was smaller than 10^{-8} m^2/s^2. After that we simulated the shaking of the system by assuming the belt to undergo harmonic oscillations according to equation (1) above. At least 9×10^4 initial time-steps were discarded in order to reach a steady state and averages were evaluated from at least 9×10^4 subsequent time-steps. All our simulations were made with $N = 200$ and the length of the segment representing the belt was $L = 20\langle d \rangle$. Tests done with N and L half as large give qulitatively similar results.

3. Results and discussion.

In all calculations the value of the Young modulus was kept constant $Y = 10^3 g\langle m \rangle/\langle d \rangle$, where $\langle m \rangle$ is the mass of a grain of diameter $\langle d \rangle$. A relatively small value of Y was chosen to allow for the use of a more convenient time-step for the numerical integration. We believe this not to be critical for the results of the simulation. Indeed, some auxiliary calculations have indicated that the Young modulus has only a weak influence on the final results as long as its value remains larger than $Y > 500g\langle m \rangle/\langle d \rangle$.

Before starting our discussion, let us first emphasize, that the movement of the belt in the vertical z direction creates an elastic restoration force (see Eq. (2)), acting against gravity. No similar force is associated to the movement of the belt in the x-direction. The particles feel this movement only *via* the shear friction term (Eq. (4)) in the equation of motion. Thus, the value of the coefficient $\gamma_{\rm s}$ controls the efficiency of the bead-transport along the belt.

The behaviour of the system was examined by plotting snapshots of the generated configurations and the trajectories of the particles. We have also computed the local number densities $\langle \rho(z) \rangle$ and transport velocities, $\langle v_x(z) \rangle$ as functions of the distance z measured from the actual position of the vibrating belt, with a grid size $\langle d \rangle$. Moreover, we evaluated the total average velocity per particle, V_x. This quantity gives the average speed (flux) of the beads along the belt. In order to check if the steady state has been reached, we have examined the velocity profiles and the total velocities V_x. When these quantities remained practically unchanged, we started to monitor the data and to calculate averages over time. Note that the periodic boundary conditions help to reach the steady state faster.

Figure 1 presents the total average velocity per particle V_x as a function of the vibration frequency, evaluated for different values of the parameters characterizing the system, whereas figures 2 and 3 show local system properties: in figure 2 we have a comparison of local densities $\langle \rho(z) \rangle$ and in figure 3, of local horizontal velocities $\langle v_x(z) \rangle$.

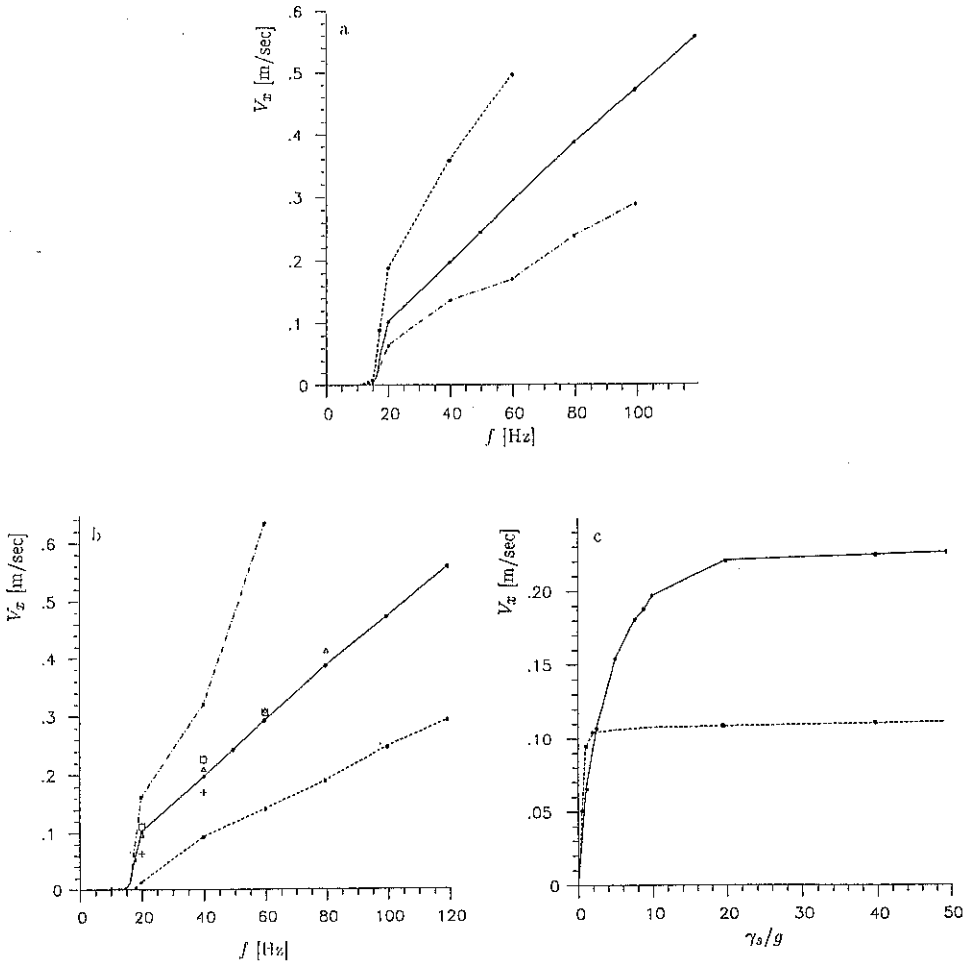

Fig. 1. — a) The flux V_x as a function of the frequency f. The calculations were carried out for $\gamma = \gamma_s = 50g$, $A_z = \langle d \rangle$, $\alpha = \pi/3$ (dash-dotted line) $\alpha = \pi/4$ (solid line) and $\alpha = \pi/6$ (short-dashed line). b) The velocity V_x against frequency for $\gamma = \gamma_s = 50g$, $\alpha = \pi/4$ and for $A_z = 1.5\langle d \rangle$ (dash-dotted line), $A_z = \langle d \rangle$ (solid line) and $A_z = 0.5\langle d \rangle$ (short-dashed line). The points were evaluated for $A_z = \langle d \rangle$, $\alpha = \pi/4$ and for $\gamma = 0$, $\gamma_s = 50g$ (triangles), $\gamma = \gamma_s = 10g$ (crosses) and $\gamma = 50g$, $\gamma_s = 100g$ (squares). c) The dependence of V_x on the shear friction coefficient, evaluated for $f = 50$ Hz (solid line) and for $f = 20$ Hz (dashed line). The remaining parameters were: $\alpha = \pi/4$, $A_z = \langle d \rangle$ and $\gamma = 50g$.

Depending on the applied vibrations, the system can exhibit a solid-like, or a liquid-like behaviour. When the excitation exceeds some level, the system starts to flow. A global characteristic of this flow is the velocity V_x. We thus begin with the discussion of the influence of model parameters on the velocity V_x - see figure 1.

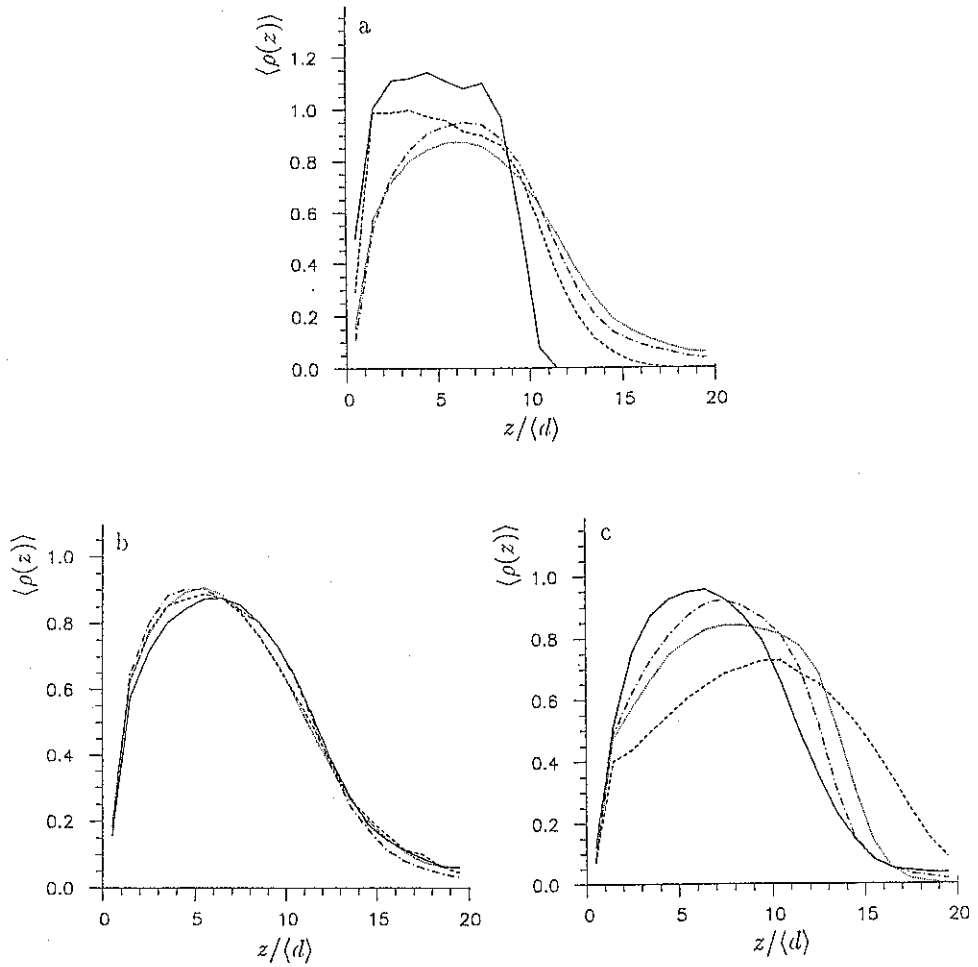

Fig. 2. — Local number densities. a) Dependence on frequency. The subsequent lines were evaluated for the frequencies: 10Hz (solid lines), 20 Hz (dashed lines), 60 Hz (dash-dotted lines) and 80 Hz (dotted line). The values of the parameters were: $\gamma = \gamma_s = 50g$ and $\alpha = \pi/4$, $A_z = \langle d \rangle$. b) Dependence on the angle of vibration. The subsequent curves were calculated for $\alpha = \pi$ (dotted line), $\pi/3$ (dash-dotted line), $\pi/4$ (solid line) and $\pi/6$ (the short-dashed line). In all cases $f = 60$ Hz, $A_z = \langle d \rangle$ and $\gamma = \gamma_s = 50g$. c) Dependence on the friction coefficients. The short-dashed line: $\gamma = \gamma_s = 10g$, the dash-dotted line: $\gamma = 0$, $\gamma_s = 50g$ and the solid line: $\gamma = 50g$ and $\gamma_s = 100g$. In all cases $\alpha = \pi/4$, $A_z = \langle d \rangle$ and $f = 80$ Hz.

All the curves of V_x *versus* f presented in figures 1a and 1b exhibit similar behaviour: after a rather rapid jump the flux increases monotonically with the frequency and at large frequencies seems to grow linearly. Interesting is, however, that in all cases the beads start to flow at about the same frequency of 16 Hz, independent of the angle α. In addition, for the investigated range

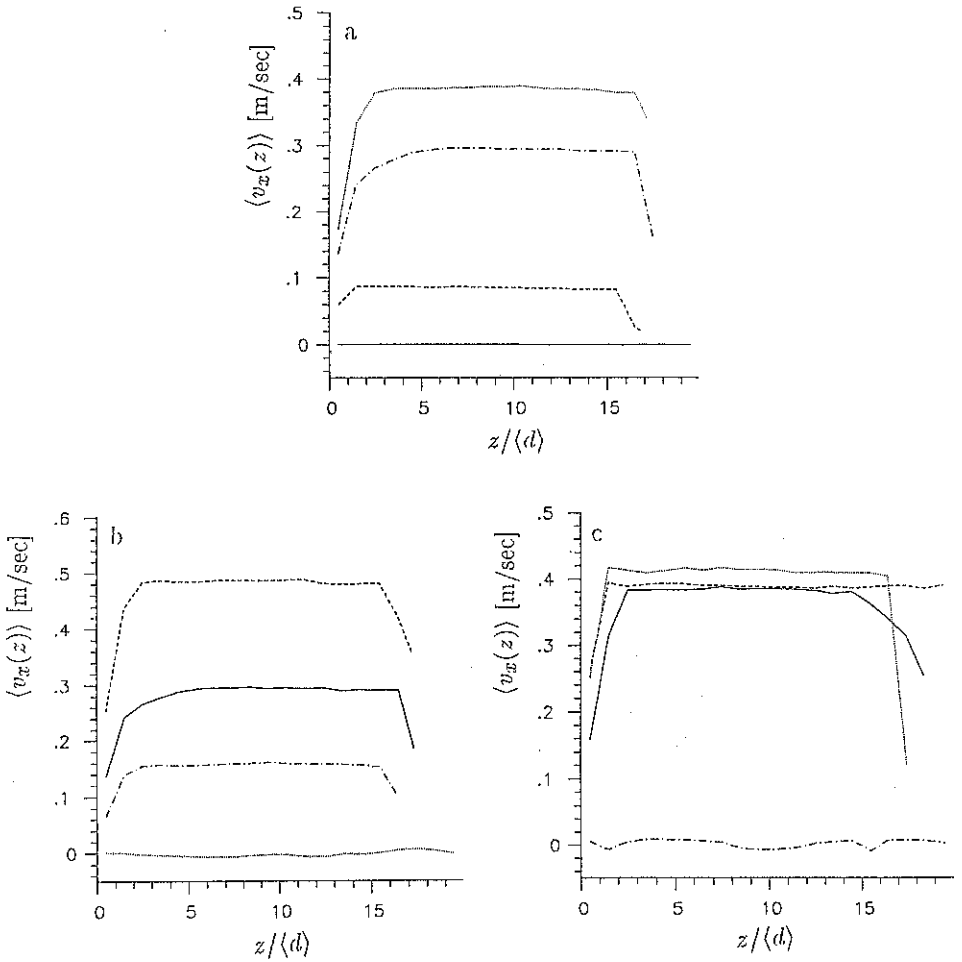

Fig. 3. — Average velocities $\langle v_x(z)\rangle$ plotted against z. The calculations were carried out for the same parameters the local densities given in figure 2 and the abbreviations of the curves are identical to those in figure 2.

of γ and $\gamma_s > g$, the transition from non-flow to flow seems to be independent of the friction coefficients. Obviously, for $\gamma_s = 0$ there is no x-component momentum transfer from the belt to the beads and the flow stops (for small values of $\gamma_s < g$ the statistics of V_x is poor). Figure 1c shows the dependence of V_x on the shear friction coefficient γ_s, for two different frequencies, namely 20 and 50 Hz. Up to $\gamma_s = 10g$ the flux increases rapidly, but a further increase of γ_s only leads to a very gentle increase of V_x.

For $A_z = \langle d\rangle = 1$ mm the frequency of the vibration at which the flow begins corresponds to a coefficient [2] $\Gamma = 4\pi^2 f^2 A_z/g$ close to 1. For a higher amplitude, $A_z = 1.5\langle d\rangle$, the flow

still starts at about $f = 16$ Hz ($\Gamma \simeq 1.5$ at this frequency) and at $f = 15$ Hz the velocity V_x is almost zero. When the amplitude is equal to $0.5\langle d\rangle$, the flow begins at a slightly higher frequency of about 18 Hz, corresponding to $\Gamma \simeq 0.8$. We should stress, however, that errors are rather big and it is difficult to evaluate the onset of the flow accurately.

Close to the belt the local density is very small. Only at low frequency the local number density shows a plateau extending up to larger z values, which ends, almost abruptly at a distance $z = 9\langle d\rangle$ from the vibrating belt (see Fig. 2a). When the frequency increases, the maximum of the local density decreases and the whole density profile becomes more smeared out. The tails observed at large heights in figure 2 indicate the existence of particles in a gas-like state above the free surface of the packing. It is interesting, that the density profile remains almost unchanged when the angle of vibrations changes - all the curves given in figure 2b collapse and the difference between them is smaller than the statistical errors. This means that the vertical component of the vibration determines almost completely the vertical density of the beads, and that the influence of the parallel component is quite small. When the friction coefficients decrease, the layer of beads becomes more smeared out (cf. Fig. 2c). Only very close to the belt the profiles seem independent of the friction. It is difficult, however, to predict how the changes of the ratio of both friction coefficients exactly influences the density profiles.

The plots of the velocity profiles $\langle v_x(z)\rangle$, i.e. the average velocity per particle, corresponding to the already discussed density profiles are displayed in figure 3. They all exhibit a well-developed plateau, showing that almost all particles move at the same speed as one would expect. The decrease of the velocity directly at the wall is due obviously to wall-particle collisions. The decrease at large heights, corresponding to the small densities, is attributed to the fact that steady state is probably not yet reached at the highest layers, since for those particles the transfer of momentum is much less efficient due to their much rarer collisions. We have checked this by also starting the simulation with all particles moving at a higher initial speed. Then the velocity of the particles decreases with time until reaching the steady state. The dashed line in figure 3c is an example of what happens: the tail at large heights disappears. Obviously, the velocity increases with increasing frequency and decreasing angle of vibrations. For $\gamma_s = 0$ the velocity $\langle v(z)\rangle$ is zero, as expected, but for $\gamma_s \geq 50g$ the velocity profile depends only very weakly on the shear friction coefficient (cf. Fig. 3c).

During real experiments it is difficult to monitor the motion of the individual particles. This, however, can be quite easily investigated in computer simulations. In figure 4 we display the trajectories of the molecules during one cycle of shaking. Examples of snapshots of particle configurations, evaluated at the begining of the vibrational cycle are given in figure 5.

When the frequency is low enough (see Figs. 4a) all the beads move synchronously along elliptic trajectories. The tilting angle of these trajectories increases with the angle of vibrations. When the shear friction coefficient γ_s becomes smaller, the tilting angle tends to $\pi/2$, provided that the vibration frequency is low enough - cf. figure 4b. When the beads start to flow, the character of their trajectories changes: at not too high frequencies they move along sinusoidal curves (Fig. 4c). With increasing frequency, the trajectories become flater and at the highest frequencies we observe a stream of particles flowing together (Fig. 4d). A decrease of the angle of vibrations makes this stream-like motion more pronounced. A similar effect is caused by increasing the friction coefficients. If, however, the shear friction coefficient γ_s is zero, the beads move essentially vertically - see figure 4e.

At quite low frequencies, the whole block of the beads moves together, following the movement of the belt. An example of a snapshot of such a configuration is given in figure 5a. Quite similar snapshots are obtained at that frequency for other values of the friction coefficients. Obviously, the angle of vibration influences the direction of the instant velocities. When the frequency increases, we first observe a "fluidization" at the upper surface of the packing. Some

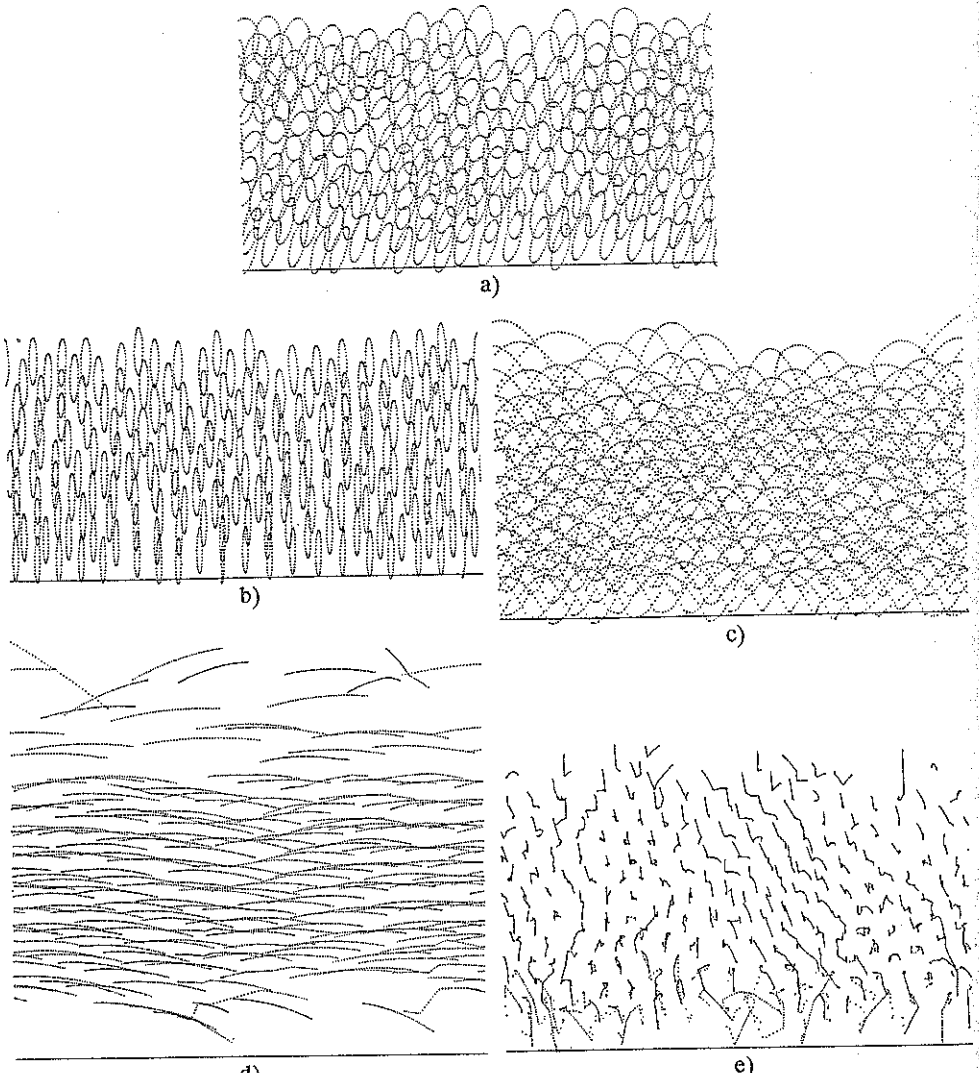

Fig. 4. — The trajectories of the particles during a single cycle of the vibration in the steady state. The trajectory of each particle is plotted after every 50 time-steps. The plots were obtained for $A_z = \langle d \rangle$, and a) $\alpha = \pi/4$, $f = 10$ Hz and $\gamma = \gamma_s = 50g$; b) $\alpha = \pi/4$, $f = 10$ Hz $\gamma = 50g$ and $\gamma_s = g$; c) $\alpha = \pi/4$, $f = 20$ Hz and $\gamma = \gamma_s = 50g$; d) $\alpha = \pi/4$, $f = 80$ Hz $\gamma = \gamma_s = 50g$; e) $\alpha = \pi/4$, $f = 80$ Hz $\gamma = 50g$ and $\gamma_s = 0$; The horizontal line denotes the average belt position.

surface particles jump, and sometimes these jumps are big. With further increase of the frequency the surface fluidization becomes more pronounced, the average density of the packing decreases (cf. also the density profiles given in Fig. 2), manifesting itself by the presence of

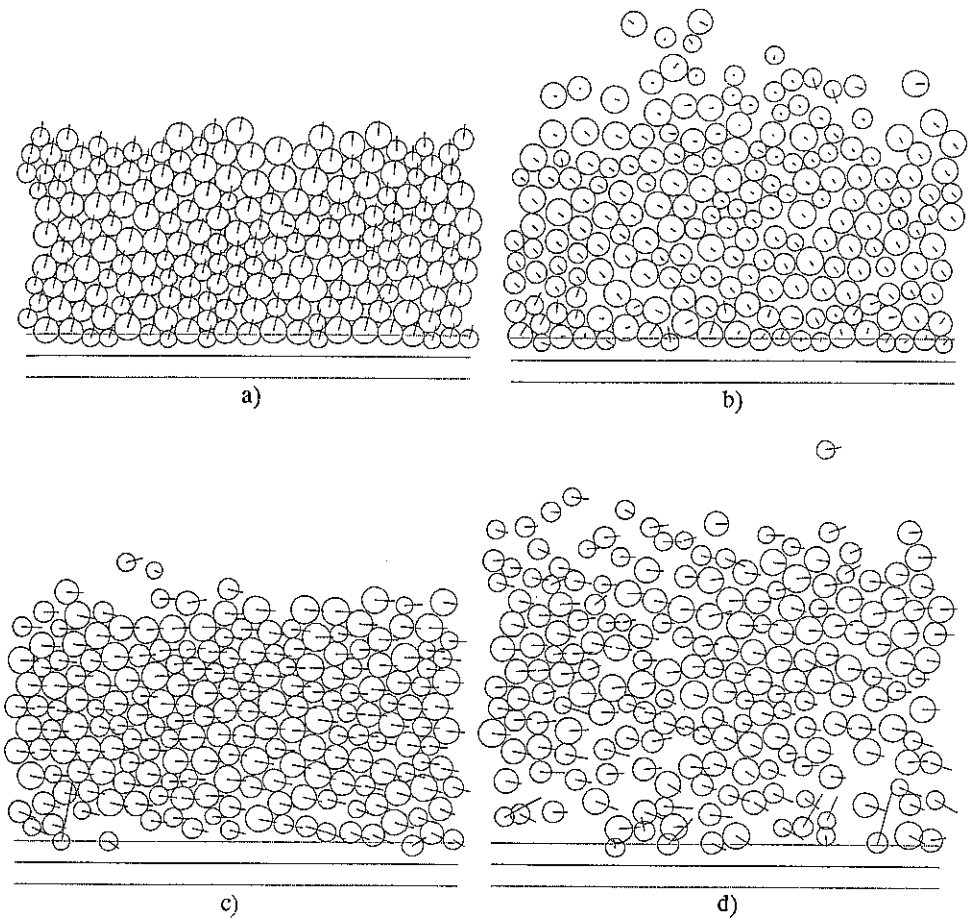

Fig. 5. — Snapshots of the configurations of particles. The dotted horizontal lines denote the maximum and the minimum position of the belt, and the solid line is its average position. The circles represent the particles and the linear segments beginning at the centres of particles indicate their instantaneous velocities. All snapshots were made at the beginning of the vibrational cycle. The plots were obtained for $A_z = \langle d \rangle$ and a) $\alpha = \pi/3$, $f = 10$ Hz $\gamma = \gamma_s = 50g$; b) $\alpha = \pi/6$, $f = 40$ Hz $\gamma = \gamma_s = 10g$; c) $\alpha = \pi/4$, $f = 100$ Hz $\gamma = \gamma_s = 50g$; d) $\alpha = \pi/4$, $f = 100$ Hz $\gamma = g$ and $\gamma_s = 50g$.

holes in the packing (see Fig. 5b). It is difficult to see this on a single picture, but observing step by step the generated snapshots, we were able to see denser regions, moving through the system. This phenomenon is more pronounced immediately after starting to vibrate, before a steady state is reached, and corresponds to the occurence of density waves in the system.

For frequencies usually higher than 60 Hz a big void develops at the bottom of the container and almost no molecules are present within the strip $[-A_z, A_z]$ (see Fig. 5c). The presence of this big void directly at the vibrating belt is very typical at higher frequencies. At the same time, when the friction coefficients are larger, the layer becomes more compact. For lower

values of the friction coefficients, however, the average density of the layer decreases (see Fig. 5d). Obviously, these features can also be identified in the plots of the local densities, given in figure 2.

We conducted a second series of numerical experiments to check how a circular obstacle inserted into the system influences the movement of the beads. To this end, a fixed circular body non interacting with the vibrating belt, was inserted at ($x = L/2$, $z = A_z$). The diameter of this obstacle was changed from $d_o = 0.1\langle d\rangle$ to $d_o = 2.5\langle d\rangle$. All the parameters characterizing the interactions of the obstacle with the beads were the same as in the case of bead-bead interactions. Note that due to the periodic boundary conditions, the obstacle in repeated along the belt.

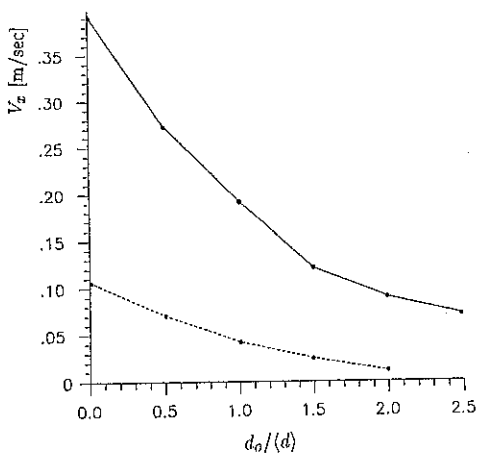

Fig. 6. — Dependence of the velocity V_x on the diameter d_o of a circular object. The calculations were carried out for $A_z = \langle d\rangle$, $\alpha = \pi/4$, $\gamma = \gamma_s = 50g$ and $f = 80$ Hz (solid line) and $f = 20$ Hz (dashed line).

Even the presence of a rather small obstacle rapidly slows down the flow. This is illustrated in figure 6 where one sees the flux as a function of d_o for 20 and 80 Hz. In figure 7 we have presented the trajectories (Fig. 7a) and a snapshot (Fig. 7b) of the beads for an obstacle of $d_o = 1.5\langle d\rangle$. Without any obstacle, the picture of the flow is that given in figure 4d. When the obstacle is inserted, the character of the motion of particles changes and the trajectories displayed in figure 7a become rather like the trajectories displayed in figure 4c, i.e. corresponding to significantly lower frequencies. Also at $f = 20$ Hz the character of the motion is changed - cf. figures 7c and 4c. Despite the big changes in the particle trajectories, even a significant obstacle does not cause turbulence in the flow at higher frequencies. We cannot treat the obstacle as only locally influencing the flow, because its initially very local effect spreads to the entire system, leading to completely different trajectories as compared to a non-perturbed system. This point is especially visible by comparing figures 7c and 4c.

We have investigated granular media on a vibrating conveyor belt which constitutes a means of transportation that is characteristic for granular media. In our simulations we used a very

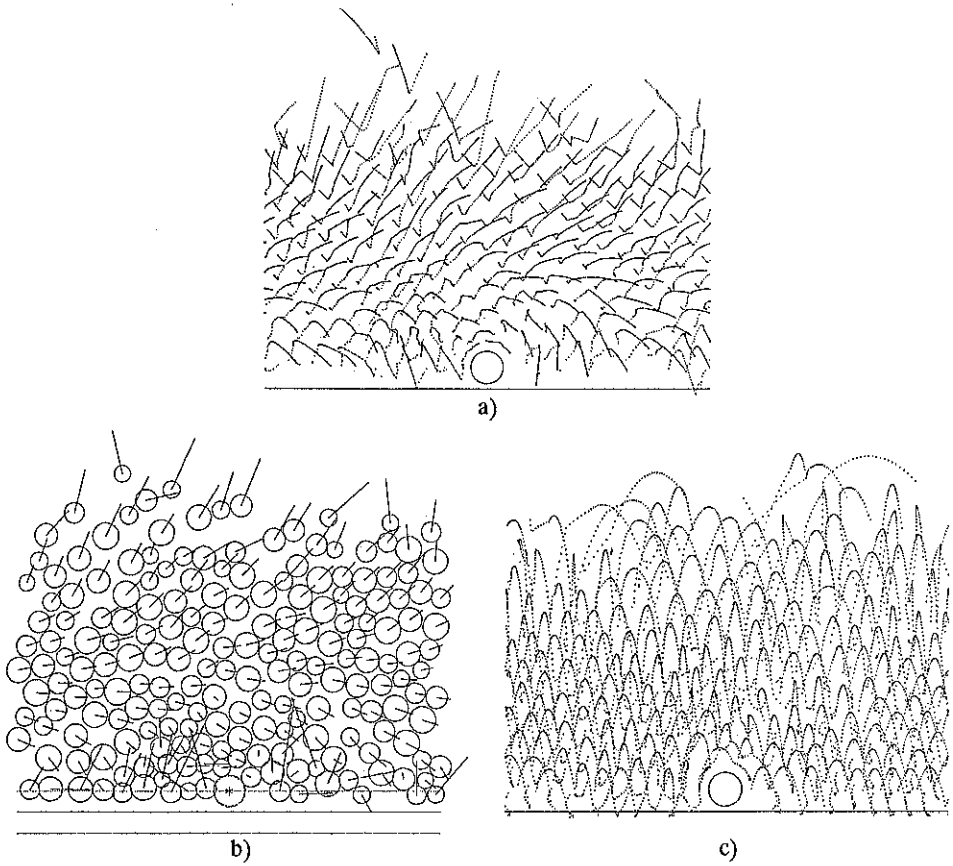

Fig. 7. — Trajectories (a and c) and snapshot (b) of the particles flowing in the presence of an obstacle. In all cases $A_z = \langle d\rangle$, $\alpha = \pi/4$, $d_o = 1.5\langle d\rangle$, $\gamma = \gamma_s = 50g$. In (a) and (b) the frequency was 80 Hz, whereas in (c) 20 Hz. The obstacle of diameter $d_o/\langle d\rangle = 1.5$ is indicated by a circle.

simplified model which only takes into account dissipation and shear friction but we think that these ingredients are enough to grasp the essential features of the granular flow. We found a rather sharp frequency threshold below which the material does not move. Above this threshold a characteristic density profile is built up which is, however, independent on the horizontal vibration of the belt. This later one determines the average velocity of the material. The shear friction coefficient only plays a role at small velocities. Any small, fixed obstacle causes long range disturbances in the whole flow patterns.

We have presented predictions that could rather easily be checked experimentally. The two friction parameters γ and γ_s are at this stage phenomenological since the detailed microscopic mechanisms are not known. For this reason we believe that the neglect of Coulomb friction, static friction, the rotation and shapes of particles etc. are not so relevant at this stage. It would of course be interesting to include these effects as well as to perform three dimensional simulations in order to check the validity of our model. In addition, the effect of more compli-

cated forms of periodic vibrations is also of interest. We hope to report on these effects in the near future.

Acknowledgements.

We thank C. Moukarzel for very useful comments. JACG is a Senior Research Fellow of the CPNq(Brazil).

References

[1] Faraday M., *Philos. Trans. R. Soc. London* **52** (1831) 299.
[2] Evesque P. and Rajchenbach J., *Phys. Rev. Lett.* **62** (1989) 44; *C. R. Acad. Sci. Ser. 2* **307** (1988) 1; **307** (1988) 223.
[3] Laroche C, Douady S. and Fauve S., *J. Phys. France* **50** (1989) 699.
[4] Rajchenbach J, *Europhys. Lett.* **16** (1991) 149.
[5] Walker J., *Sci. Am.* **247** (1982) 167.
[6] Dinkelacker F., Hübler A. and Lüscher E., *Biol. Cybern.* **56** (1987) 51.
[7] Baxter G. W., Behringer R. P., Fagert T. and Johnson G. A., *Phys. Rev. Lett.* **62** (1989) 2825.
[8] Williams J.C., *Powder Techn.* **15** (1976) 245.
[9] Rosato A., Strandburg K.J., Prinz F. and Swendsen R.H., *Phys. Rev. Lett.* **58** (1987) 1038; *Powder Techn.* **49** (1986) 59.
[10] Devillard P, *J. Phys. France* **51** (1990) 369.
[11] Haff P.K. and Werner B.T., *Powder Techn.* **48** (1986) 239.
[12] Reynolds O., *Philos. Mag. S.* **20** (1885) 469.
[13] Drake T. G., *J. Geophys. Res.* **95** (1990) 8681.
[14] Johnson P. C. and Jackson R., *J. Fluid Mech.* **150** (1985) 67.
[15] Savage S. B., *J. Fluid Mech.* **92** (1979) 53.
[16] S.F. Edwards and R.B.S. Oakeshott, *Physica A* **157** (1989) 1080.
[17] Edwards S. F., *J. Stat. Phys.* **62** (1991) 889.
[18] Mehta A. and Edwards S. F., *Physica A* **157** (1989) 1091.
[19] Baxter G.W. and Behringer R.P., *Phys. Rev. A* **42** (1990) 1017; *Physica D* **51** (1991) 465.
[20] Caram H. and Hong D.C., *Phys. Rev. Lett.* **67** (1991) 828.
[21] Hanes D. M. and Inman D. L., *J. Fluid Mech.* **150** (1985) 357.
[22] Jaeger H.M., Chu-heng Liu, Nagel S. R. and Witten T. A., *Europhys. Lett.* **11** (1990) 619.
[23] Bagnold R. A., *Proc. Roy. Soc. London A* **295** (1966) 219.
[24] Campbell C.S., *Ann. Rev. Fluid Mech.* **22** (1990) 57.
[25] Tagushi Y.-h., preprint.
[26] Ristow G., *J. Phys. I France* **2** (1992) 649.
[27] Hong D.C. and McLennan, preprint.
[28] Thompson P. A. and Grest G. S., *Phys. Rev. Lett.* **67** (1991) 1751.
[29] Campbell C.S. and Brennen C. E., *J. Fluid Mech.* **151** (1985) 167.
[30] Meakin P. and Jullien J., *Physica A* **180** (1992) 1.
[31] Gallas J.A.C., Herrmann H.J and Sokołowski S., preprint HLRZ 5/92.
[32] Gallas J.A.C., Herrmann H.J and Sokołowski S., preprint HLRZ 8/92.
[33] Clement E. and Rajchenbach J., *Europhys. Lett.* **16** (1991) 133.
[34] Schmidt H. and Peschl I., *Fördern u. Heben* **15** (1965) 606.
[35] Tildesley D., Computational Physics, R.D. Kenway and G.S. Pawley Eds., NATO Advanced Study Institute (Edinburgh University Press, 1987).
[36] Tildesley D.J. and Allen M.P. Computer Simulations of Liquids, (Oxford University Press, Oxford 1987).